different substances. These results are unexpectedly good because predicted values for D_c from Equation (21) are not very accurate. Equation (22) and Figure 3 are recommended to be used for liquids having acentric factors between 0.2 and 0.4, but as it is seen from Table 4, even for some substances having $\omega > 0.4$, the results are satisfactory. Evidently most liquids of interest have $0.2 < \omega < 0.4$

Note that in Table 4 for ethanol, if the extrapolated value of D_c is used instead of the predicted value from Equation (21), the error will be reduced from 25 to 0.0%. Therefore, extrapolated values for D_c are more preferable to the predicted values from Equation (21). Unfortunately, for many liquids, data for diffusivity in the range of critical temperature were not available. It should be emphasized that one of the reasons for having a large error for ethanol is the high value for its acentric factor.

NOTATION

a, a' = constants
b, b', b'' = constants
D = self-diffusion coefficient, m^2s
D_c = self-diffusion coefficient at critical temperature
D_r = reduced self-diffusion coefficient
g_c = gravitational constant
h = Planck's constant
K = thermal conductivity, J/m·s°K
k = Boltzman's constant
M = molecular weight
m = proportionality constant
N = Avogadro's number
P = pressure
R = gas constant
T = temperature, °K
T_b = normal boiling point, °K
T_c = critical temperature, °K
t = time
V = liquid molar volume
v_s = velocity of sound, m/s

Greek Letters

α = proportionality constant
β = proportionality constant
γ = heat capacity ratio
ω = acentric factor
μ = absolute viscosity, N·s/m²
μ_F = viscosity based on force unit
μ_c = viscosity at critical temperature, N·s/m²
ϕ = density

LITERATURE CITED

Bird, R. B., W. E. Stewart and E. N. Lightfoot, *Transport Phenomena*, Wiley, New York (1960).

Dullien, F. A. L., "Prediction Equations for Self-Diffusion in Liquids: A Different Approach," *AIChE J.*, **18**, 62 (1972).

Graboski, M. S., and W. C. Braun, Private Communication, Penns. State Univ., University Park (1968).

Li, J. C. M., and P. Chang, "Self-Diffusion Coefficient and Viscosity in Liquids," *J. Chem. Phys.*, **23**, 518 (1955).

Loflin, T., and E. McLaughlin, "Diffusion in Binary Liquid Mixtures," *J. Phys. Chem.*, **73**, 186 (1969).

McCall, D. W., and D. C. Douglas, "Diffusion in Binary Solutions," *ibid.*, **71**, 987 (1967).

McLaughlin, E., "Viscosity and Self-Diffusion in Liquids," *Trans. Faraday Soc.*, **55**, 28 (1959).

Perry, J. H., *Chemical Engineer's Handbook*, 4 ed., McGraw-Hill, New York (1963).

Skelland, A. H. P., *Diffusional Mass Transfer*, Wiley, New York (1974).

Smith, J. M., and H. C. Van Ness, *Introduction to Chemical Engineering Thermodynamics*, 3 ed., McGraw-Hill, New York (1975).

Manuscript received April 3, 1979; revision received October 1, and accepted October 11, 1979.

Dynamics of Bubbles and Entrained Particles in the Rotating Fluidized Bed

RENE CHEVRAY*

YAU NAM I. CHAN

and

FRANK B. HILL

Department of Energy and Environment
Brookhaven National Laboratory
Upton, New York 11973

Trajectories of bubbles and entrained particles in the rotating fluidized bed were obtained from equations expressing a balance among inertial, centrifugal, Coriolis, gravity and drag forces. The solutions led to information on the behavior of isolated bubbles, bubble swarms and the elutriation characteristics of the rotating fluidized bed.

SCOPE

In a rotating fluidized bed, the bed particles are located in a rotating cylindrical container having a porous wall. A stable fluidized bed results from a balance of centrifugal forces arising from rotation and drag forces caused by gas entering the vessel through its porous wall. The minimum fluidization velocity increases with rotational speed and is usually large when compared with that for the familiar gravitational bed in which the earth's gravitational force opposes the gas drag force. For this reason, the rotation bed has been proposed as a high capacity gas-solid contactor for application in areas such as the processing of particulate foods and combustion of gas, oil and coal. It has also been suggested for use in propulsion in outer space, where gravity forces are small.

Rene Chevray is a visiting scientist. Permanent address: Department of Mechanical Engineering, State University of New York at Stony Brook, Stony Brook, NY 11794.

Knowledge of the fluid dynamic behavior of rotating fluidized beds is at present essentially limited to information on minimum fluidization conditions. The present work is concerned with the theory of the behavior of bubbles and entrained particles in the rotating system. It was undertaken as a preliminary to studies of the transport and reaction properties of such systems.

Bubble and entrained particle behavior were determined from the solution of equations expressing a balance among inertial, centrifugal, Coriolis, gravity and drag forces.

CONCLUSIONS AND SIGNIFICANCE

When viewed in a frame of reference rotating with the bed, an isolated small bubble followed a radial path from its point of release toward the bed center. Its velocity was accurately predicted by a modification of the expression of Davies and Taylor (1950) for the rise of a spherical cap bubble in an inviscid liquid. The modification consisted of replacing the gravitational acceleration by the local radial acceleration. Significant deflections from a radial path existed for large bubbles due to Coriolis forces. At low rotational speeds, bubble rise was large. Bubble swarm velocities and volume became large in the inner portion of thick beds, suggesting spontaneous bubble generation there and a loss of coupling with the outer portions of the bed.

The fate of single particles injected into the freeboard region depended on their size. Large particles were returned to the bed, while small particles were elutriated. Particles of intermediate size were retained in circular orbits in the freeboard.

In a comparison of the elutriation properties of rotating and gravitational beds, it was found as a first approximation that particles of the same size were elutriated from both beds but at a flow rate in the rotating bed which was greater than that in the gravitational bed by the ratio of the radial to gravitational accelerations.

The findings reported are useful as background for experimental study of bubble and entrained particle motion and for the study of the transport and reaction properties of rotating fluidized beds.

Many phenomena occurring in gas fluidized beds are importantly influenced by the two-phase nature of these systems. Chemical reaction behavior, heat and mass transfer processes and solids mixing and entrainment phenomena have all been related to the presence and action of bubbles and a dense gas-solid phase.

Thus far, studies of two-phase behavior have been concerned with the familiar gravitational fluidized bed in which gravity acts to oppose the drag force on the bed particles. In the present paper, certain of these studies are carried out for a rotating fluidized bed. In this kind of bed (see Figure 1), particles are held against the wall of a cylindrical vessel by centrifugal force and are fluidized by a gas entering the vessel through the porous wall. The rotating fluidized bed has been considered recently as the basis for a nuclear reactor for propulsion in outer space (Ludewig et al., 1974), for processing of particulate food materials (Brown et al., 1972) and as a high capacity combustor (Levy et al., 1976; Metcalfe and Howard, 1977; Demircan et al., 1978).

In this paper, theoretical analyses of the motion of bubbles and entrained particles in the rotating fluidized bed are presented. Details are given elsewhere (Chevray et al., 1979). The results may be of some interest in interpreting the two-phase nature of this device and in particular of the effect of replacing the gravity force by a combination of centrifugal, Coriolis and gravitational forces in a gas fluidized system. The centrifugal and Coriolis forces can be varied by changing the rotational speed and can be made arbitrarily large compared to gravity.

FLUID DYNAMIC FEATURES OF THE BED AND FREEBOARD REGIONS

In the bed proper, no measurements of the velocity distribution have been made. However, it seems reasonsable to assume that at and slightly above the minimum fluidization velocity, the shear stresses imparted by the distributor will propagate inward rapidly so that the bed will come very quickly into solid body rotation. At high fluidization velocities, motions of large bubbles could possibly induce nonsolid body types of velocity distributions. As we will see later, the work of Donaldson and Snedeker (1962), for example, suggests that it is the ratio of the tangential to radial components of momentum which dictates the nature of the flow field. In the bed region, the tangential component is much larger than the radial, due mainly to the difference between the densities of the solid particles and the gas. This situation would tend to favor maintenance of solid body rotation except at very high velocities. An exception to this statement will be found later in the paper, where it is suggested that nonsolid body rotation may exist in the inner portions of thick rotating fluidized beds, even at low fluidizing velocities.

At low rotational speeds, the inner free surface of the bed takes the stable shape of a paraboloid of revolution (Levy and Chen, 1978). For sufficiently high rotational speeds, the bed region can be considered to be a cylindrical annulus.

In the freeboard region, the gas emerging from the bed surface is moving radially inward and is moving tangentially owing to rotation. Immediately adjacent to the bed, constant angular momentum is maintained in the gas so that the tangential component of velocity varies in inverse proportion to the radius. This zone is in irrotational motion, much like that in a free vortex. Toward the center of the freeboard, the high velocities cannot be sustained, and the flow regime changes to rotational (forced vortex), allowing dissipation to occur. The combined resulting flow is that of a Rankine vortex, and the relative extent of the two zones is determined by several factors. For a given geometry, the most decisive one is probably the ratio of tangential to radial initial components of momentum.

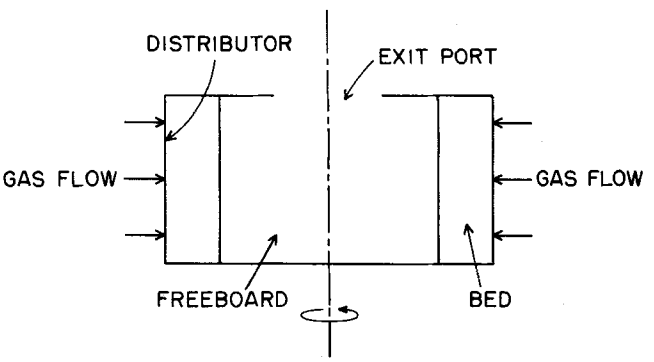

Figure 1. Rotating fluidized bed.

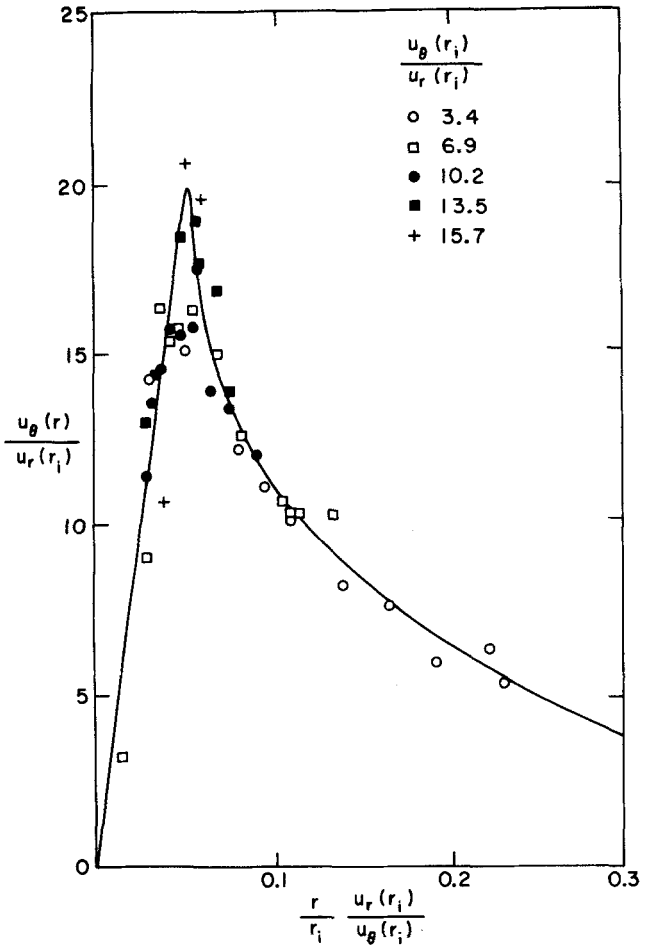

Figure 2. Universal representation of the tangential velocity distribution derived from data of Donaldson and Snedeker.

The higher this ratio, the greater the extent of the rotational core, and, conversely, the smaller this ratio, the higher the extent of the free vortex region.

For present purposes, we obtained a quantitative description of the magnitude and location of the maximum tangential velocity in a Rankine vortex from the data of Donaldson and Snedeker (1962). These authors reported tangential velocity distributions in a porous rotating cylindrical vessel completely open at the top. Gas entered through the porous wall and left through the open top. We found that if we plotted their data for tangential-to-radial velocity ratios at the vessel wall greater than 3* in the form $u_\theta(r)/u_r(r_i)$ vs. (r/r_i) $[u_r(r_i)/u_\theta(r_i)]$, then a single curve, independent of velocity ratio could be obtained, as shown in Figure 2. The equation describing this empirical relationship in the viscous core is

$$\frac{u_\theta(r)}{u_r(r_i)} = 400 \cdot \frac{u_r(r_i)}{u_\theta(r_i)} \cdot \frac{r}{r_i} \tag{1}$$

and the position of the maximum is given by

$$\frac{r_m}{r_i} = 0.05 \cdot \frac{u_\theta(r_i)}{u_r(r_i)} \tag{2}$$

It is assumed here that the exit port radius is equal to r_m. From the work of Roschke (1966) on vortex flows in a vessel with a partially closed top, it appears that for small values of the bed length-to-diameter ratios, the locations of the exit port and maximum tangential velocity are nearly coincident.

In the irrotational region of the vortex, there is probably a sink for angular momentum near the top and bottom due to the lower rotational speeds there. The resulting secondary flow is very likely too complex to analyze in detail, so we assume that the flow is without end effects.

The tangential component of the velocity distribution in the viscous core of the freeboard region is obtained from Equation (1) after we substitute in this equation the following equations for $u_r(r_i)$ and $u_\theta(r_i)$:

$$u_r(r_i) - \frac{Q}{2\pi r_i h} \tag{3}$$

$$u_\theta(r_i) = \omega r_i \tag{4}$$

One obtains for $u_\theta(r)$

$$u_\theta(r) = \frac{100\,Q^2}{\omega\pi^2 r_i^4 h^2} r,\ 0 \le r \le r_m \tag{5}$$

In the irrotational region

$$u_\theta(r) = \frac{\omega r_i^2}{r},\ r_m \le r \le r_i \tag{6}$$

This latter equation has the required $1/r$ form and satisfies the boundary conditions at $r = r_m$ and $r = r_i$.

We assume the vertical component of the velocity distribution in the freeboard region to have the following form:

$$u_z(z) = \frac{Q}{\pi r_m^2 h} z,\ 0 \le r \le r_m \tag{7}$$

$$= 0,\ r_m \le r \le r_i \tag{8}$$

The linear variation of $u_z(z)$ with height indicated in Equation (7) is in good agreement with the observations of Turner (1966).

The radial component of the velocity distribution in the viscous core region is obtained by substituting the expressions for the partial derivatives of u_θ [Equation (5)] and u_z [Equation (7)] with respect to θ and z, respectively, in the continuity equation and integrating the result. One obtains

$$u_r(r) = -\frac{Q}{2\pi r_m^2 h} r,\ 0 \le r \le r_m \tag{9}$$

In the irrotational region, it is assumed that

$$u_r(r) = -\frac{Q}{2\pi r h},\ r_m \le r \le r_i \tag{10}$$

In summary, the velocity distribution in the forced vortex region is given by Equations (5), (7) and (9) and in the free vortex region by Equations (6), (8) and (10).

BUBBLE MOTION

Isolated Bubbles

Bubbles manifest themselves in rotating fluidized beds in much the same way they do in stationary beds, by the appearance of moving void volumes adjacent to a transparent bounding surface of a bed or by the growth and bursting of convex caps at the free surface of a bed. Other than qualitative observations such as these, no information of an experimental nature on bubbles in rotating fluidized beds is available. The only theoretical observation is that of Murray (1965) who has shown that the rotating system, like the gravitational system, is unstable with respect to small density perturbations when the solid-to-fluid phase density ratio is large.

Studies have been made, however, of bubble motion in rotating liquids. These are of interest to the present topic because of the expected similarity of gas bubble behavior in rotating gas-solid and liquid systems. This similarity is well known in gravitational systems (Davidson and Harrison, 1963).

Theoretical treatments of the motion of single isolated bubbles in rotating liquids have been given by Clifton et al. (1969), Schrage and Perkins (1972), Catton and Schwartz (1972) and Siekmann and Dittrich (1975). It was of interest to these workers to determine the path of a bubble within a rotating liquid as it passed toward the axis of rotation from its point of release. In particular, it was of interest to determine for a reference frame

* A transition in flow regime occurs at $u_\theta(r_i)/u_r(r_i) \sim 3$. This transition, as mentioned by Donaldson and Snedeker (1962), is due to a change in flow regime from a one-celled to a two-celled structure. For the illustrative examples given later in the paper, this ratio is greater than 5, and the use of the correlation of Figure 2 is therefore justified.

rotating with the liquid the deflection from a purely radial path resulting from the Coriolis force, and to determine the variation in bubble speed along the bubble path. The problem was generally solved by assuming the bubbles to retain constant size throughout their path and to treat them effectively as particles, setting up and solving the appropriate equations of particle dynamics. In each of the above papers, the problem was solved in two dimensions. Different assumptions were made from one treatment to another regarding the influence of gravity. The orientation of the axis of rotation when specified was usually taken to be horizontal. In the present paper, the equations are given in three dimensions for the situation in which the axis of rotation is vertical, corresponding to the arrangement found in the rotating fluidized bed, and interest is centered on the large spherical cap bubbles found in fluidized beds. We assume the treatment is valid for single isolated bubbles in rotating fluidized beds as well as in rotating liquids, but in presenting the derivation reference is made only to the rotating liquid.

Consider a bubble released at the outer radius r_o of a rotating cylinder of liquid. The force balance equations governing the motion of the bubble, written for a frame of reference rotating with the liquid, are as follows:

Inertial force		Centripetal force	Coriolis force	Gravitational force	Drag force
$(M + M_0)(\ddot{r} - r\dot{\theta}^2)$	=	$-M_0\frac{\rho}{\rho'}\omega^2 r$	$-M_0\frac{\rho}{\rho'}2r\omega\dot{\theta}$		$-\frac{1}{2}\rho\pi r_e^2\lvert\underline{u}_b\rvert\dot{r}C_D$
$(M + M_0)(2\dot{r}\dot{\theta} + r\ddot{\theta})$	=		$-M_0\frac{\rho}{\rho'}(-2\omega\dot{r})$		$-\frac{1}{2}\rho\pi r_e^2\lvert\underline{u}_b\rvert r\dot{\theta}C_D$ (11)
$(M + M_0)\ddot{z}$	=			$M_0\frac{\rho}{\rho'}g$	$-\frac{1}{2}\rho\pi r_e^2\lvert\underline{u}_b\rvert\dot{z}\,C_D$

where

$$\lvert\underline{u}_b\rvert = (\dot{r}^2 + r^2\dot{\theta}^2 + \dot{z}^2)^{\frac{1}{2}} \tag{12}$$

The angle θ is taken positive in the counter clockwise direction, and z is positive upward. The basic assumptions used in writing Equations (11) are that $\rho' << \rho$ and that the bubble retains constant shape and volume during its motion.

As indicated on the left-hand side of Equations (11), the mass undergoing acceleration includes M_0, the mass of the bubble, and M, the added liquid mass (Batchelor, 1970), where for spheres

$$M = \frac{1}{2}\frac{\rho}{\rho'}M_0 \tag{13}$$

The centripetal and Coriolis forces are felt through a modification of the pressure field set up in the fluid in much the same way as the distribution of hydrostatic pressure is responsible for buoyancy. Corresponding forces and, of course, the gravity force are therefore proportional to the mass of the displaced liquid. The components of the drag force act opposite in direction to the inertial force. It is assumed that there are no accelerative effects on the drag coefficient. The effective bubble dimension in the drag force term is taken to be the radius r_e of a sphere with a volume equal to that of the spherical cap bubble. As already mentioned, the bubble is assumed to retain constant shape and volume. With regard to the assumption of constant volume, it will be seen later that the speed of the bubble is approximately proportional to the square root of the bubble radius and hence to the one sixth power of its volume. Thus, change in volume can have little effect on speed.

The drag force terms in Equations (11) may be written in terms of the mass of the gas bubble, since

$$M_0 = \frac{4}{3}\pi r_e^3\rho' \tag{14}$$

Upon making this substitution in Equations (11) and neglecting M_0 compared to M, we obtain

$$\ddot{r} - r\dot{\theta}^2 = -2(\omega^2 r + 2r\omega\dot{\theta}) - \frac{3}{4}\frac{C_D}{r_e}\lvert\underline{u}_b\rvert\dot{r},$$

$$2\dot{r}\dot{\theta} + r\ddot{\theta} = 4\omega\dot{r} - \frac{3}{4}\frac{C_D}{r_e}\lvert\underline{u}_b\rvert r\dot{\theta}, \tag{15}$$

$$\ddot{z} = 2g - \frac{3}{4}\frac{C_D}{r_e}\lvert\underline{u}_b\rvert\dot{z}$$

Immediately evident is the fact that if ρ' is much smaller than ρ, as has been assumed in the present work, then neither ρ nor ρ' plays a role in the motion of the bubble.

Equations (15) can be expressed in terms of the following dimensionless variables:

$$\begin{aligned} R &= r/r_o, \\ \Theta &= \theta/\omega t_o, \\ Z &= z/r_o, \\ T &= t/t_o, \\ \alpha &= \omega^2 r_o/g, \\ \beta &= \frac{3}{4}C_D\frac{r_o}{r_e} \end{aligned} \tag{16}$$

A definition of t_o is required. One similar to that of Clifton et al. (1969) is used:

$$t_0 = \beta^{\frac{1}{2}}/\omega \tag{17}$$

In terms of these variables, Equations (15) become

$$\left.\begin{aligned} \ddot{R} - \beta R\dot{\theta}^2 &= -2\beta R(1 + 2\dot{\theta}) - \beta(\dot{R}^2 + \beta R^2\dot{\theta}^2 + \dot{Z}^2)^{\frac{1}{2}}\dot{R}, \\ 2\dot{R}\dot{\theta} + R\ddot{\theta} &= 4\dot{R} - \beta(\dot{R}^2 + \beta R^2\dot{\theta}^2 + \dot{Z}^2)^{\frac{1}{2}}R\dot{\theta}, \\ \ddot{Z} &= 2\beta/\alpha - \beta(\dot{R}^2 + \beta R^2\dot{\theta}^2 + \dot{Z}^2)^{\frac{1}{2}}\dot{Z} \end{aligned}\right\} \tag{18}$$

Initial conditions are

$$\left.\begin{aligned} T = 0,\ R = 1,\ Z = 0,\ \theta = 0, \\ \dot{R} = \dot{R}_o,\ \dot{Z} = 0,\ \dot{\theta} = 0 \end{aligned}\right\} \tag{19}$$

Equations (18) subject to these initial conditions were integrated numerically.

The results of the integration are shown for a range of values of β for $\alpha = 10$ in Figure 3 and for $\alpha = 100$ in Figure 4. Trajectories are shown in the $R-\theta$ plane in the upper part of these figures and in the R-Z plane in the lower part. Trajectories in a full cylinder of liquid are shown. It was found that the trajectories were insensitive to the initial velocity $\dot{R}_o$ for the range of β values considered. In inspecting these figures, it is useful to keep in mind values of β which are physically meaningful. For spherical cap bubbles, C_D is a constant equal to 2.6 (Haberman and Morton, 1953). If interest is restricted to values of $r_o/r_e \geq 5$, then $\beta = 3/4\ C_D\ r_o/r_e \geq \sim 10$.

Trajectories in the $R-\theta$ plane are similar to those reported by Clifton et al. (1969) and show that for small bubbles and/or for large cylinders ($\beta \geq 100$), the Coriolis force produces little departure from a purely radial path. For large bubbles ($\beta < 100$), the departure becomes significant. Very nearly the same trajectories are found for $\alpha = 10$ and $\alpha = 100$. Trajectories in the R-Z plane for $\alpha = 10$ (Figure 3) show that the action of the gravitational force leads to appreciable bubble rise and that the rise increases with increasing bubble size as expected. Bubble rise is considerably less for $\alpha = 100$.

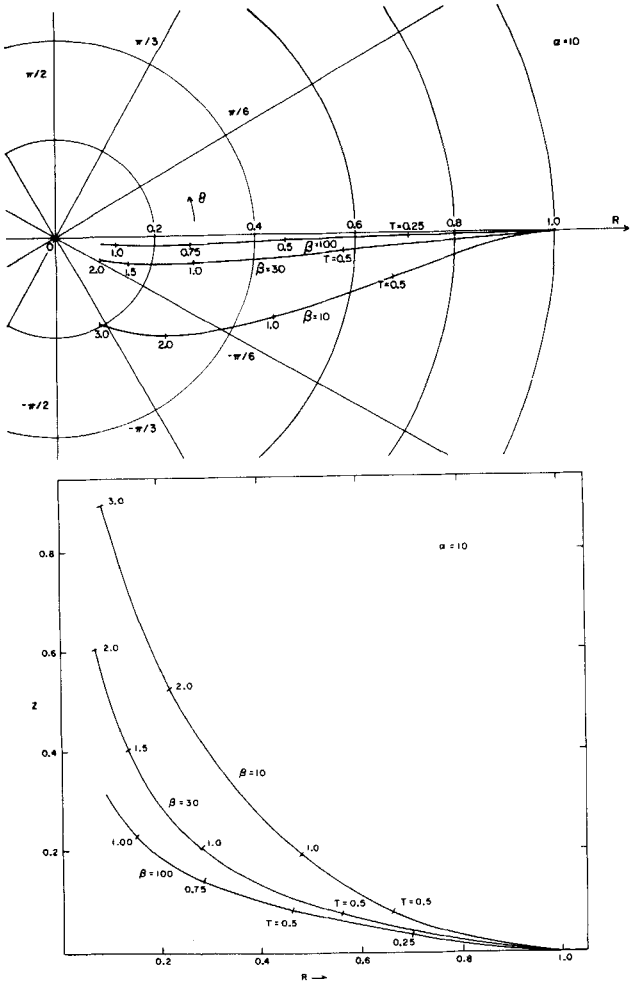

Figure 3. Dimensionless representation of the trajectories of isolated bubbles in a rotating liquid. $\alpha = 10$. Dimensionless times of travel $T = \omega t/\beta^{\frac{1}{2}}$ are indicated on each curve.

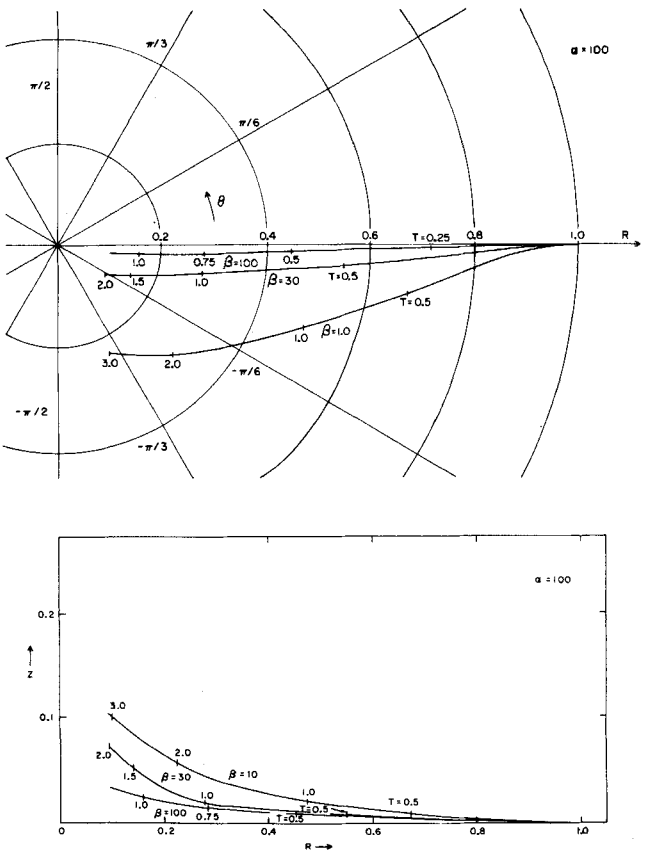

Figure 4. Dimensionless representation of the trajectories of isolated bubbles in a rotating liquid. $\alpha = 100$. Dimensionless times of travel $T = \omega t/\beta^{\frac{1}{2}}$ are indicated on each curve.

Because β is not a function of ω but t_o is dependent on ω, the trajectories do not depend on rotational speed, but the bubble speed along these trajectories does vary with rotational speed and is, in fact, linearly proportional to ω. The speed along the paths is not constant, as may be seen from the values of T given along the paths.

For conditions under which the Coriolis deflection is small, it may be determined (Chevray et al., 1979) as expected that the bubble velocity predicted through the above approach agrees well with a modified Davies and Taylor (1950) calculation. The modification consists of replacing the acceleration due to gravity by the local radial acceleration.

Swarm of Bubbles

We discuss the speed of a swarm of bubbles under conditions such that Coriolis and buoyancy deflections are negligible, that is, for small bubbles at high rotational speeds. Under these circumstances, one may show in a manner similar to that for gravitational beds (Davidson and Harrison, 1963) that the radial speed of a swarm of bubbles at the radial position r is

$$u_b(r) = u(r) - u_{mf}(r) + u_{b\infty}(r) \tag{20}$$

or, since

$$u(r) = u(r_o)\,(r_o/r) \tag{21}$$

$$u_b(r) = u(r_o)\,(r_o/r) - u_{mf}(r) + u_{b\infty}(r) \tag{22}$$

The minimum fluidization velocity, $u_{mf}(r)$, is obtained from a correlation similar to that of Wen and Yu (Richardson, 1971):

$$N_{Re_{mf}}(r) = 25.7\,[\sqrt{1 + 5.531 \times 10^{-5} N_{Ga}(r)} - 1] \tag{23}$$

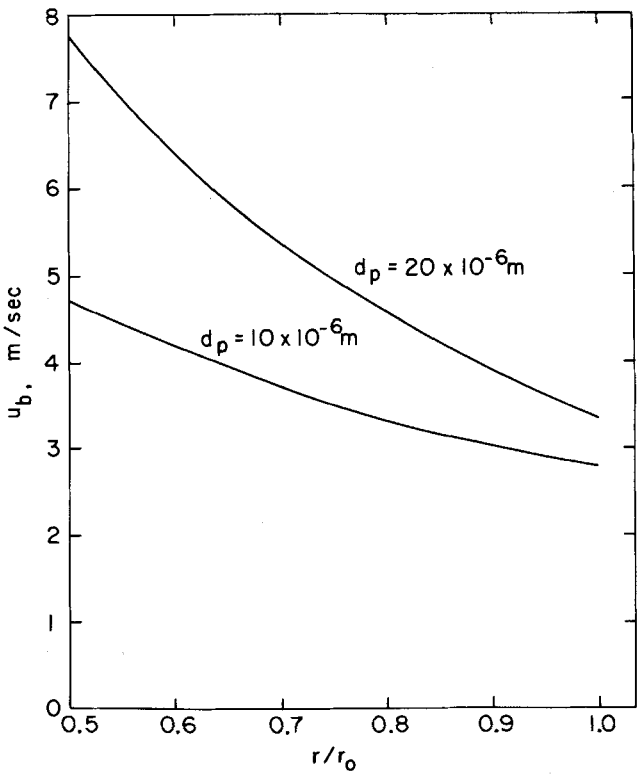

Figure 5. Velocity of swarm of bubbles in a rotating fluidized bed. $r_o = 0.125$ m, $r_i = 0.0625$ m, $\rho = 2\,000$ kg/m^3, $\rho' = 1$ kg/m^3, $\nu = 2 \times 10^{-5}$ m^2/s, $r_r = 0.006$ m, $u(r_o) = 2\,u_{mf}(r_o)$, $a_r(r_o) = 9\,800$ m/s^2.

where

$$N_{Re_{mf}}(r) = d_p U_{mf}(r)\rho/\mu \tag{24}$$

$$N_{Ga}(r) = \frac{\rho_g(\rho_s - \rho_g)d_p^3\omega^2 r}{\mu^2} \tag{25}$$

The isolated bubble velocity, $u_{b\infty}(r)$, is given by the modified Davis and Taylor expression

$$u_{b\infty}(r) = 1.01\ \omega(r\ r_e)^{\frac{1}{2}} \tag{26}$$

The swarm velocity, $u_b(r)$, was evaluated using Equations (26) and (23) in Equation (22). Illustrative calculations were made for a bed with the following parameters: $r_o = 12.5 \times 10^{-2}m$; $r_i = 6.25 \times 10^{-2}m$; $\alpha = 100$, $d_p = 100 \times 10^{-6}$, $200 \times 10^{-6}m$; $\rho = 2\ 000\ kg/m^3$; $\rho' = 1\ kg/m^3$. The results are shown in Figure 5 for a fluidizing velocity at the outer radius equal to twice the minimum. There it is seen that for both particle sizes, the swarm velocity increases with decreasing radial position. This behavior is in contrast to the velocity of the isolated bubble which decreases with decreasing radial position. The swarm velocity increases because the local fluidization velocity, $u(r)$, dominates in Equation (22) for the example chosen. The velocity of the isolated bubble would tend to dominate at larger bubble sizes and larger radial positions, reversing the direction of variation of swarm velocity with radius just shown. Thus this dependence must be examined in each case.

According to the usual notions about the two-phase nature of gas fluidization, the fraction of gas passing through the bed as bubbles is $[u(r) - u_{mf}(r)]/u(r)$. A plot of this quantity vs. r is shown in Figure 6 for $100 \times 10^{-6}\ m$ particles in the same bed used in the example in Figure 5. Two values of the fluidization velocity at the outer bed radius were considered: the minimum and twice the minimum. For both cases, the fraction of gas in the bubble phase increases markedly as the radius decreases, suggesting spontaneous bubble generation as the gas passes through the bed. Consideration of coalescence or splitting is neglected in making this observation. The high fraction of gas as bubbles at small radii calls into question the assumption of solid body rotation in the bed at these locations. A loss of coupling with the rotating system is suggested in the inner regions of thick beds.

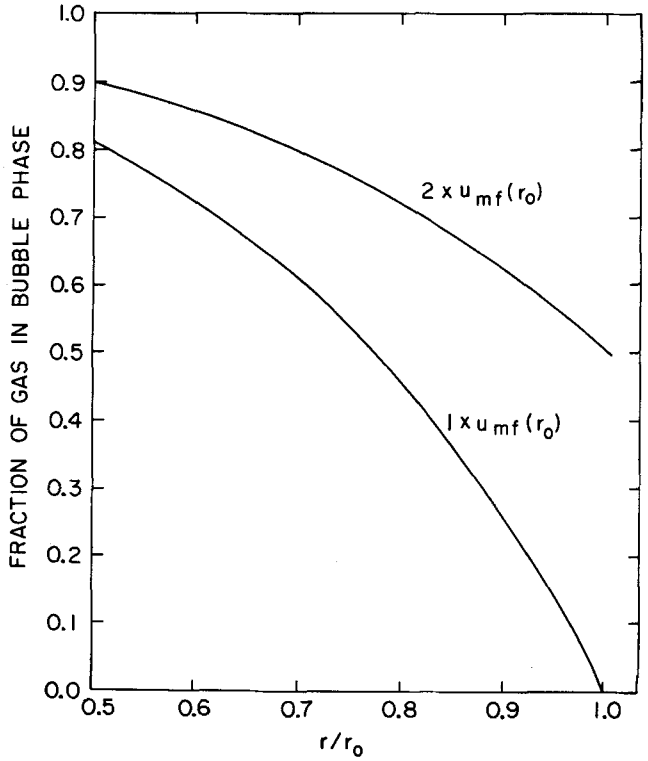

Figure 6. Fraction of gas in bubble phase for a swarm of bubbles in a rotating fluidized bed. Parameters are the same as those for Figure 5 except $d_p = 100 \times 10^{-6}$ m and $u(r_o) = 1 \times u_{mf}(r_o)$ and $2 \times u_{mf}(r_o)$.

PARTICLE MOTION IN THE FREEBOARD REGION

We consider the fate of particles ejected singly into the freeboard region. Particles there are acted upon by centrifugal force tending to return them to the bed. The drag force, on the other hand, acting in the direction of the gas velocity relative to the particle, tends to bring them toward the center. Finally, for a frame of reference rotating with the bed, the Coriolis force acts on the particles in such a way as to tend to displace them in a direction normal to their relative velocity and in the direction of rotation.

The drag force on the particles is expressed as

$$F_D = \frac{1}{2}\rho'|\underline{U}|^2 A C_D \tag{27}$$

C_D is a function of Reynolds number, and for the range of interest $N_{Re} < 100$ can be expressed by

$$C_D = \frac{24}{N_{Re}} + \frac{4.6}{N_{Re}^{0.38}} \tag{28}$$

This expression was obtained by the authors as the best fit to the experimental results of Haberman and Morton (1953) in this Reynolds number range.

With the above considerations in mind, the complete equations of motion of the center of mass of a particle can be written as

$$\begin{aligned} \ddot{r} - r\dot{\theta}^2 &= \omega^2 r + 2r\omega\dot{\theta} - BC_D|\underline{U}|U_r, \\ 2\dot{r}\dot{\theta} + r\ddot{\theta} &= -2\omega\dot{r} - BC_D|\underline{U}|U_\theta, \\ \ddot{z} &= -g - BC_D|\underline{U}|U_z \end{aligned} \tag{29}$$

where

$$B = \frac{3}{8}\frac{\rho'}{\rho}\frac{1}{r_p} \tag{30}$$

$$N_{Re} = \frac{2r_p|\underline{U}|}{\nu} \tag{31}$$

In these equations, we have neglected the added mass of the particle which is very much smaller than the particle mass. In contrast to the equations describing the motion of a large bubble, density does play a role in the case of particle motion. Also, the drag coefficient is now a function of Reynolds number.

The three components of the relative particle velocity used in the above equations may be obtained from Equations (5) to (10):

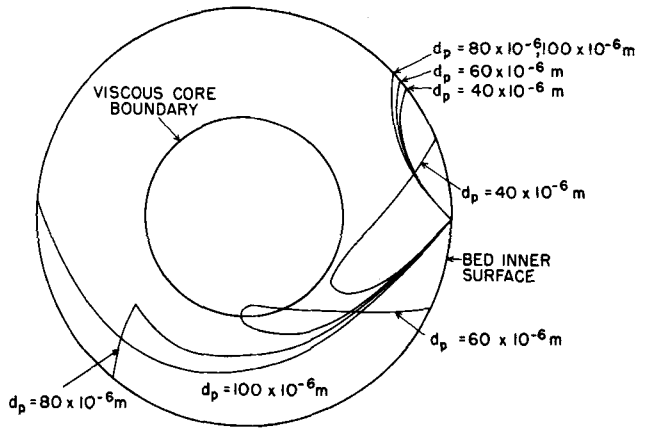

Figure 7. Trajectories of entrained large particles in the freeboard of a rotating fluidized bed. Angles of release = $\pi/4$, $3\pi/4$ rad. Particle diameters = 40×10^{-6}, 60×10^{-6}, 80×10^{-6}, 100×10^{-6}m. Parameters common to Figures 7 through 11: $r_o = 0.125$ m, $r_i = 0.075$ m, $\rho = 2\ 000$ kg/m^3, $\rho' = 1$ kg/m^3, $\nu = 2 \times 10^{-5}$ m^2/s, $r_e = 6 \times 10^{-2}$ m, $u(r_o) = 2u_{mf}(r_o)$, $\omega = 60$ rad/s.

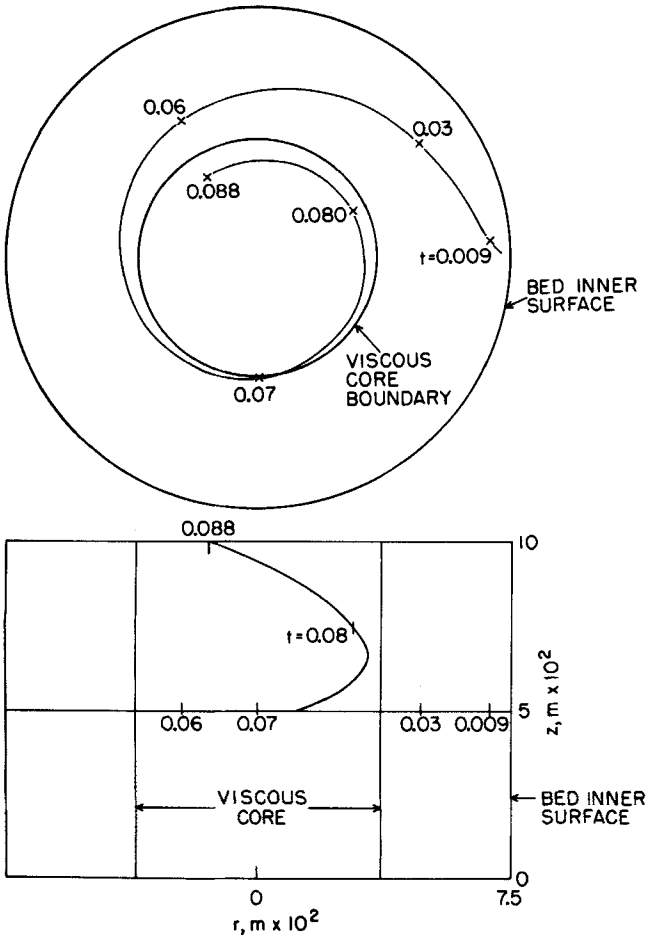

Figure 8. Trajectory of small particle in the freeboard of a rotating fluidized bed. Angle of release = $\pi/2$ rad. Particle diameter = 6×10^{-6} m. Emission height = 5×10^{-2} m. $h = 10 \times 10^{-2}$ m. Travel time in s is indicated on each curve. For other parameters see Figure 7 caption.

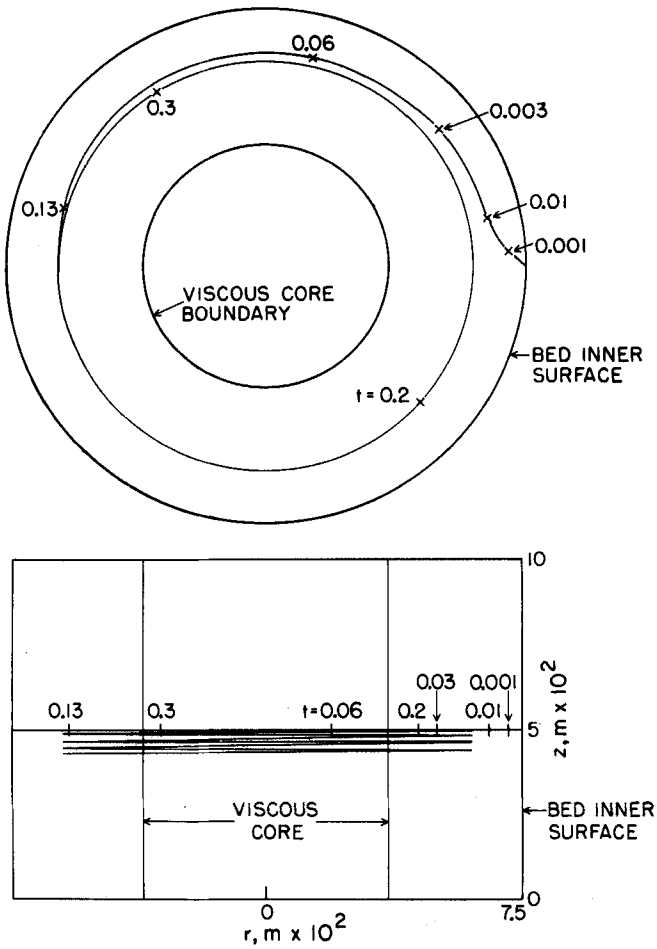

Figure 9. Trajectory of particle of intermediate size in freeboard of a rotating fluidized bed. Angle of release = $3\pi/4$ rad. Particle diameter = 15×10^{-6} m. Travel time in s is indicated on each curve. For other parameters see Figure 7 caption.

$$U_r = \frac{Q}{2\pi r_m^2 h} r + \dot{r}$$

$$U_\theta = -\frac{100Q^2 r}{\pi^2 \omega r_i^4 h^2} + \omega r + r\dot{\theta} \quad 0 \le r \le r_m, \tag{32}$$

$$U_z = \dot{z} - \frac{Q}{\pi r_m^2} \cdot \frac{z}{h}$$

$$U_r = \frac{Q}{2\pi r h} + \dot{r}$$

$$U_\theta = -\frac{\omega r_i^2}{r} + \omega r + r\dot{\theta} \quad r_m \le r \le r_i \tag{33}$$

$$U_z = \dot{z}$$

The above system of second-order differential equations, Equations (29), was solved numerically for several typical conditions. A method for integration of stiff differential equations developed by Chan et al. (1978) was used to provide satisfactory results for small particles.

The following parameters were used in illustrative calculations: $r_o = 12.5 \times 10^{-2}$m, $r_i = 7.5 \times 10^{-2}$m, $h = 10 \times 10^{-2}$m, $\omega = 60$ rad/s, $\rho = 2\,000$ kg/m^3, $\rho' = 1$ kg/m^3, $u(r_0) = 2u_{mf}(r_0)$, $r_e = 6 \times 10^{-2}$m. The bed was assumed to be made up of 100×10^{-6} m diameter particles. The fate of particles of this and smaller sizes was examined. Particles were given initial velocities with vertical and horizontal components equal to those of an isolated bubble reaching the inner bed surface. Initial angular orientation of the particles with respect to the bed surface was assumed to be in the range $\pi/4$ to $3\pi/4$ rad.

The resulting trajectories are shown in Figures 7 to 9. Bed rotation direction is counter clockwise. The time of travel in seconds is indicated in most of these figures. Particles with diameters ranging from 100×10^{-6} m down to 40×10^{-6} m are seen in Figure 7 to return ultimately to the bed, with those initially inclined in the direction of rotation returning via a more direct route. Rapid return of entrained particles to a rotating bed has been reported by Demircan et al. (1978). Particle rise is significant for particles which pass through the central core where they encounter gas with an upward velocity component. Such was the case for the 60×10^{-6} m particle shown in Figure 7. It returned to the bed at a point approximately 2.1×10^{-2} m higher than its point of ejection. Particles which did not pass through the core rose approximately 2×10^{-3} m. Thus, 60×10^{-6} m particles ejected within 2×10^{-2} m of the top of the bed would be elutriated, whereas larger and smaller particles in the 20×10^{-6} to 100×100^{-6} m range would return to the bed unless they were ejected within 1×10^{-3} to 2×10^{-3} m of the bed top.

Small particles are elutriated from the bed as shown for 6×10^{-6} diameter particles in Figure 8. At first, the particles rise slowly (not noticeable in the figure) under the influence of initial conditions. Then they fall slowly owing to gravity (also not noticeable). Finally, they rise with the flow toward the exit with a helical trajectory.

The trajectory of a particle of intermediate size (15×10^{-6} m diameter) is shown in Figure 9. Such particles are captured and would remain in circular orbit were it not for the effect of gravity which leads to a slow spiraling toward the bottom of the bed container. For particles of intermediate size, initial trajectories were a function of initial ejection direction, but the final orbit was not.

The existence of three classes of particles in the sense just described was implied in the discussion of elutriation properties

of a rotating fluidized bed given by Levy et al. (1976).

For particles captured in the irrotational flow region, the radial component of the drag force must be balanced by the centrifugal force. One can show that the radial acceleration in this region is given by

$$a_r(r) = \omega^2 \frac{r_i^4}{r^3} \tag{34}$$

Hence, the centrifugal force on a particle is

$$F_c = \frac{4}{3} \pi r_p^3 \rho \omega^2 \frac{r_i^4}{r^3} \tag{35}$$

For sufficiently small particles, the drag force may be evaluated using Stokes law. When a balance of forces is written and the resulting equation is evaluated at $r = r_i$, it is found that

$$d_p^2 = 18\ \nu \frac{\rho'}{\rho} \frac{u_r(r_i)}{a_r(r_i)} \tag{36}$$

This equation gives the minimum size of particle which would be retained by the bed and, for present purposes, may be considered to be the maximum size elutriated. A similar expression can be derived for the maximum size of particle elutriated from a gravitational bed:

$$d_p^2 = 18\ \nu \frac{\rho'}{\rho} \cdot \frac{u}{g} \tag{37}$$

To a first approximation, we may compare the elutriation properties of the rotating and gravitational fluidized beds by comparing these two very similar equations, Equations (36) and (37). The fluidizing velocities, $u(r_i)$ and u, may be evaluated using Equation (23). According to this latter equation, at small accelerations, the fluidizing velocity is linearly proportional to the acceleration for either bed. Thus the maximum size of particle elutriated is independent of acceleration and is the same for both beds. The throughput in the rotating system, however, is higher by the ratio, $a_r(r_i)/g$.

ACKNOWLEDGMENT

The authors express appreciation to Robert Pfeffer who read an early version of the manuscript and made valuable suggestions. This work was supported by the Division of Chemical Sciences, U.S. Department of Energy, Washington, D.C., under Contract No. EY-76-C-02-0016.

NOTATION

A = cross-sectional area of particle in plane normal to relative gas flow direction
a = acceleration
a_r = radial acceleration
B = constant equal to $3/8\ \rho'/\rho\ 1/r_p$
C_D = drag coefficient
d_p = particle diameter
F_D = drag force
g = acceleration due to gravity
h = height of bed
M = added mass of gas bubble
M_0 = mass of gas bubble
N_{Ga} = Galileo number $= \rho'(\rho - \rho')\ d_p^3\ a/\mu^2$
N_{Re} = particle Reynolds number $= d_p\ u/\nu$
$N_{Re_{mf}}$ = particle Reynolds number at minimum fluidization $= d_p\ u_{mf}/\nu$
Q = volumetric flow rate of gas
r = radial position
r_e = radius of sphere having a volume equal to that of bubble
r_i = inner radius of fluidized bed
r_m = position of maximum in tangential velocity distribution in freeboard; corresponds to radius of exit port
r_o = outer radius of fluidized bed
r_p = particle radius
R = r/r_o
R_c = radius of curvature of bubble at bubble nose
t = time
t_o = $\beta^{\frac{1}{2}}/\omega$
T = t/t_o
u = superficial fluidizing velocity
u_b = velocity of isolated bubble or of bubble swarm, according to context
u_{b-DT} = velocity of isolated bubble derived using the Davies and Taylor approach
$u_{b\infty}$ = velocity of isolated bubble
u_{mf} = superficial gas velocity at minimum fluidization
u_r = radial component of gas velocity
u_z = vertical component of gas velocity
u_θ = angular component of gas velocity
$|\underline{u}|$ = magnitude of gas velocity vector
$|\underline{U}|$ = magnitude of velocity vector of particle relative to gas
U_r = radial component of velocity of particle relative to gas
U_z = vertical component of velocity of particle relative to gas
U_θ = angular component of velocity of particle relative to gas
z = vertical position coordinate
Z = z/r_o

Greek Letters

α = $\omega^2 r_o/g$
β = $(3/4)\ (C_D)\ (r_o/r_e)$
θ = angular coordinate
Θ = $\theta/(\omega t_o)$
μ = viscosity
ν = μ/ρ'
ρ = particle density
ρ' = gas density
ω = angular speed

LITERATURE CITED

Batchelor, G. K., *An introduction to fluid dynamics*, Cambridge Univ. Press, Cambridge, England (1970).

Brown, G. E., D. F. Farkas and E. S. DeMarchena, "Centrifugal Fluidized Bed," *Food Technol.*, **26**, No. 12, 23-30 (1972).

Catton, I., and S. H. Schwartz, "Motion of Bubbles in a Rotating Container," *J. Spacecraft*, **9**, 468-471 (1972).

Chan, Y. N. I., I. Birnbaum and L. Lapidus, "Numerical Solution of Stiff Differential Equations via Imbedding Techniques," *Ind. Eng. Chem. Fundamentals*, **17**, 133-148 (1978).

Chevray, R., Y. N. I. Chan and F. B. Hill, "Dynamics of Bubbles and Entrained Particles in the Rotating Fluidized Bed," Brookhaven Natl. Lab. Rep. BNL-26082 (1979).

Clifton, J. V., R. A. Hopkins and D. W. Goodwin, "Motion of a Bubble in a Rotating Liquid," *J. Spacecraft*, **6**, 215-217 (1969).

Davidson, J. F., and D. Harrison, *Fluidized Particles*, Cambridge Univ. Press, Cambridge, England (1963).

Davies, R. M., and G. I. Taylor, "The Mechanics of Large Bubbles Rising Through Extended Liquids and Through Liquids in Tubes," *Proc. Royal Soc.*, **A200**, 375-390 (1950).

Demircan, N., B. M. Gibbs, J. Swithenback and D. S. Taylor, "Rotating Fluidized Bed Combustor," *Proc. 1978 Int'l. Fluidization Conf.*, Cambridge, England (Apr., 1978).

Donaldson, C. duP., and R. S. Snedeker, "Experimental Investigation of the Structure of Vortices in Simple Cylindrical Vortex Chambers," Aeronautical Research Associates of Princeton, Inc., Rep. No. 47 (1962).

Haberman, W. L., and R. K. Morton, "An Experimental Investigation of the Drag and Shape of Air Bubbles Rising in Various Liquids," David Taylor Model Basin Rep. No. 802 (1953).

Levy, E. K., and J. C. Chen, "Minimum Fluidization and Startup of a Centrifugal Fluidized Bed," *Proc. 1978 Int'l. Fluidization Conf.*, Cambridge, England (Apr., 1978).

Levy, E. K., C. Dodge and J. C. Chen, "Parametric Analysis of a Centrifugal Fluidized Bed Coal Combustor," ASME Paper 76HT68, presented at National Heat Transfer Conference, Boulder, Colo. (1976).

Ludewig, H., A. J. Manning and C. J. Raseman, "Feasibility of Rotating Fluidized Bed Reactor for Rocket Propulsion," *J. Spacecraft and Rockets*, **11**, No. 2, 65-71 (1974).

Metcalfe, C. I., and J. R. Howard, "Fluidization and Gas Combustion in a Rotating Fluidized Bed," *Appl. Energy*, 3, 65-74 (1977).
Murray, J. D., "On the Mathematics of Fluidization. Part I. Fundamental Equations and Wave Propagation, "*J. Fluid Mech.*, 21, 465-493 (1965).
Richardson, J. F., "Incipient Fluidization and Particulate Systems," in *Fluidization*, J. F. Davidson and D. Harrison, ed., pp. 25-64, Academic Press, New York (1971).
Roschke, E. J., "Experimental Investigation of a Confined Jet-Driven Water Vortex," Jet Propulsion Lab. Tech. Rep. No. 32-982, NASA CR 78550 (1966).
Schrage, D. L., and H. C. Perkins, Jr., "Isothermal Bubble Motion Through a Rotating Liquid," *J. Basic Eng.*, 94, 187-192 (1972).
Siekmann, J., and K. Dittrich, "Über die Bewegung von Gasblasen in einem rotierenden Medium," *Ingenieur Archiv*, 44, 131-142 (1975).
Turner, J. S., "The Constraints Imposed on Tornado-Like Vortices by the Top and Bottom Boundary Conditions," *J. Fluid Mech.*, 25, 377-400 (1966).

Manuscript received May 4, 1979; revision received October 8, and accepted October 11, 1979.

Electrically Stimulated Aerosol Filtration in Packed Beds

G. M. HARRIOTT and D. A. SAVILLE

Textile Research Institute
and,
Department of Chemical Engineering
Princeton University
Princeton, New Jersey 08540

Since charged particles are quite mobile in an electric field, charge is often added to aerosol particles to facilitate capture; indeed, provision for such charging is an indispensable part of electrostatic precipitators. Nevertheless, calculations disclose that a very slight amount of charge may suffice when the distance the aerosol particle must travel to the collector surface is small, contrary to the usual situation. In the experiments described here a model aerosol containing 0.5 μm polystyrene particles passed through a radioactive charge neutralizer to deliberately reduce the charge as much as practicable and then through a packed bed under the influence of a fairly large external electric field. Filtration efficiencies approaching 100% were obtained owing to the influence of the field on small amounts of residual charge.

SCOPE

It is well known that aerosol particles with diameters in the range 0.2 to 1 μm are difficult to remove by filtration, since such particles are too large for diffusion to be effective but are too small for efficient inertial capture. Electrical effects, however, enhance the rate of capture of such particles by three mechanisms: coulombic attraction between a charged particle and a collector, attraction between dipoles induced in a particle and a collector by an externally imposed field, and through the force on a charged particle due to an external electric field. For the capture of submicron size particles, the charged particle-electric field interaction can be especially effective. Estimates of the amount of charge required for efficient filtration using a packed bed suggest that very small amounts may suffice, and the experiments described here were used to test this hypothesis. In the experiments, the charge levels on a model aerosol were deliberately reduced using a radioactive source neutralizer. Coarse metal screens placed perpendicular to the flow were used to impose an electric field across the glass bead packing.

CONCLUSIONS AND SIGNIFICANCE

High filtration efficiencies were achieved which were due primarily to the influence of the field on a small amount of residual charge on the particles. This was deduced from the following observations and calculations. First, comparison of aerosol concentrations measured by electrical and mechanical methods indicates that the average charge level on the aerosol after passing through the neutralizer was small, close to the average of two to three elementary charges reported by Whitby and Liu (1968) for a similarly neutralized aerosol. This is also consistent with the amount necessary to produce the observed rates by the external field charged particle force which, according to the computations reported here, ranged from one to four elementary units per particle. Since, in addition to the fact that the coulombic interaction is independent of the external field, the charge levels themselves appear too small to create significant coulombic interactions, this sort of electrical effect was discounted. On the other hand, estimates of the collection rates expected from polarization effects show that this effect is weak and not the primary cause of the high capture rates observed. Finally, lower efficiencies were observed in the upper portions of the bed, and this is consistent with the effect of an external field on an aerosol with a distribution of charge. Thus, the charged particle-external field force emerges as the dominant cause of the high collection rates.

Whitby and Liu (1966) have shown that the natural average charge levels on many particles are fairly large, suggesting that the natural charge on respirable aerosols may be adequate for filtration, thereby eliminating the need for a separate charging unit in some instances. This would further reduce the operating costs for what already appears to be a very economical filter, since the pressure drop across the bed is low and the current small.

0001-1541-80-3708-0398-$00.75.

Current Address for G. M. Harriott is: Department of Chemical Engineering, Massachusetts Institute of Technology, Cambridge, Massachusetts 02139